(Received 19 February 2025, Accepted 8 April 2025, Scheduled 14 April 2025)

Graphene as a Phase Shifter Element for Reflectarray Beam-Steering at THz Frequencies

Suhail A. Qureshi[1], Muhammad R. Kamarudin[1,*], Yoshihide Yamada[2], Muhammad I. Abbasi[3,*], Muhammad H. Dahri[4], Zuhairiah Z. Abidin[1], and Nordin Ramli[5]

[1]*Faculty of Electrical and Electronic Engineering*
Universiti Tun Hussein Onn Malaysia, Batu Pahat 86400, Malaysia
[2]*Malaysia Japan International Institute of Technology*
Universiti Teknologi Malaysia Kuala Lumpur, Jalan Semarak, Kuala Lumpur 54100, Malaysia
[3]*Faculty of Electronics and Computer Technology and Engineering (FTKEK)*
Universiti Teknikal Malaysia Melaka (UTeM), Hang Tuah Jaya, Durian Tunggal, Melaka 76100, Malaysia
[4]*Department of Telecommunication Engineering*
Dawood University of Engineering and Technology, Karachi, Sindh 74800, Pakistan
[5]*MIMOS Berhad, Technology Park Malaysia, Kuala Lumpur 57000, Malaysia*

ABSTRACT: In Terahertz (THz) frequencies, using traditional phase delay components is extremely difficult, and graphene has the potential to be used in THz. Graphene is typically used at less than $\lambda/16$ dimensions. However, it can potentially change the properties of a unit cell in a reflectarray and act as an electronic phase-shifting element at $\lambda/2$ dimensions. Therefore, this paper proposes the design and application of graphene in unit cells to develop reflectarray beam steering. A metal-graphene hybrid structure is proposed in this work for designing the reconfigurable reflectarray antenna (RRA). The unit cell operating at 1.025 THz frequency consists of a thin graphene sheet as a phase-shifting element inside a golden ring, where graphene is used as the phase delay component. The variation in the chemical potential of graphene leads to changes in the reflection coefficient phase for each unit cell. A circular aperture array comprising a maximum of 489 elements shows a total of 80° beam-steering with side-lobe levels of less than −10 dB and a maximum gain of over 20 dBi. The −1 dB bandwidth of 12% was obtained at the centre frequency of 1025 GHz between 950 GHz and 1075 GHz. The aperture efficiency of the designed RRA is found to be 11%. This type of antenna could be an advent for the development of terahertz Reflecting Intelligent Surface (RIS).

1. INTRODUCTION

Reflectarray is a type of antenna that delivers high gain with a low loss, which is a major limitation encountered by a typical phased array antenna and individual reflector [1]. It combines the principles of geometrical optics and phased arrays, which, as a result, produces a predesigned far-field radiation pattern, eliminating the need for a complex feeding network. A standard structure of reflectarray consists of a combination of metasurface-based grounded resonators [2]. The phasing mechanism of a reflectarray can be obtained by designing an array of passive unit cells with individual reflection phases. The reflection phase of a unit cell typically depends on the critical dimension of the metallic patch [3]. The far-field radiation pattern of the aggregated arrangement can be shaped as desired or collimated by varying the dimensions of each unit cell. A reflectarray construction ideally requires a phase change of the unit cell to cover a 360° phase change. It is also possible to achieve a higher phase shift by using multiple metallic layers [4, 5]. However, for narrowband operation, the phase shift of 360° is sufficient.

This kind of array antenna can also be electronically reconfigured to alter its collimated phase using electronic materials or switches. A PIN diode-based practical demonstration was done in [6] to develop a reflectarray working in X-band frequencies. The 6×6 reflectarray structure based on the diode's ON/OFF configuration for each unit cell showed ±6° beam switching. Another beam-steerable reflectarray was designed in [7], which incorporated a polarization-rotating unit cell that functions as a 1-bit phase shifter. The unit cell consisted of four arrows connected to two PIN diodes. Changing the biasing of those two PIN diodes could result in a 180° phase shift with a reflection coefficient of > -2 dB. The beam steering capability was determined within the range of ±60°. Similarly, four varactor diodes were used for reconfiguring a 2.4 GHz reflectarray antenna with three-dimensional coverage in [8]. Microelectromechanical system (MEMS) technology was used in [9] for a digitally reconfigurable reflectarray antenna at 12 GHz. It should be highlighted that with the ever-increasing demand for faster link speed, the advent of the THz band offers a potential solution but presents challenges simultaneously. In [1], Liquid Crystal (LC) was employed to dynamically control the reflection phase of the reflectarray antenna operating at 115 GHz by varying the applied bias voltage. In [10], an algorithm-based

* Corresponding authors: Muhammad Ramlee Kamarudin (mramlee@uthm.edu.my); Muhammad Inam Abbasi (inamabbasi@utem.edu.my).

design and analysis of a 1-bit LC-based reflectarray was presented operating at 108 GHz. The scanning range of the reflectarray was $\pm 40^{\circ}$. A novel THz reflective phase shifter of a metal-dielectric-metal configuration was proposed in [11] using nematic liquid crystal. The orientation of LC was controlled by the applied electric field with the help of applied biasing to the LC that changes its dielectric constant. The phase shift with the application of biasing exceeded the value of 180° from 102.5 GHz to 104.3 GHz. The maximum phase shift obtained was 249 at the centre frequency. However, the operation of LC has not been reported over this range of frequencies. The phase delay components, such as PIN diode, Varactor diode, and LC, suffer from complexity in being integrated with THz antennas.

Materials varying their physical properties based on the external environment have been recently incorporated with reflectarray antenna to vary its phase. Graphene is a prime example of those materials, which was first used for designing a reflectarray antenna by Carrasco and Perruisseau-Carrier [12] in 2013. The designed graphene antenna operated at 1.3 THz. Compared to gold, a graphene-based antenna patch obtained slightly increased loss and reduced cross-polarization [12]. The better performance of graphene in the THz reflectarray than a reflectarray designed with conventional metallic patches was possible in terms of bandwidth and design simplification at the cost of increased losses [12]. However, challenges in graphene's applications in RRAs rely on controlled protocols of fabrication that enable reproducible and stable devices. Scalability and integration at the wafer scale are additional limitations. The applications of graphene are growing rapidly. It is considered a promising material for electrochemical sensors due to its 2-dimensional property and vulnerability to ambient atmosphere [13]. Graphene has also been reported recently in the modelling of reconfigurable reflectarray antenna (RRA). In [14], an RRA was modelled based on graphene, and scattering characteristics of the reflectarray were analysed in co-polarization and cross-polarization. The integration of graphene with a metallic structure was explored in [15] for THz communication. Graphene was modelled as a 2D structure along with the gold acting as a patch of the unit cell. At 1.5 THz, the losses were -27 dB, and it was found that complete phase control is possible within the common range of bias supply of graphene [15]. A remarkable contribution to the designing of a graphene-based reconfigurable reflectarray antenna was made in [16] for the generation of THz vortex waves. A graphene-based circularly polarized reflectarray was proposed for wideband operation from 1.4 THz to 1.7 THz. The periodic dimensions of the unit cell were set to 15 µm, which equals $\lambda/13$ [17]. Another graphene-based reflectarray was also proposed, where a unit cell was designed at about $\lambda/2$ dimensions [18]. The purpose of the study was to tune the operating frequency of the array. However, reported reflectarray antennas based on graphene designed on $\lambda/2$ structures have not been studied extensively for the RRA beam steering, and the capability of being used as a tunable element in the THz band remains a question. This is because graphene is a type of element that exhibits a slow-wave propagation phenomenon associated with its plasmonic modes. The unit cells involving graphene are typically designed at less than $\lambda/16$ and graphene patches at less than $\lambda/24$ because of their plasmonic mode propagation. In [19], a THz graphene unit cell was designed to operate at $\lambda/2$ dimensions for achieving a high gain of reflectarray. The single beam reflectarray demonstrated a maximum gain of 18.7 dBi at 1.5 THz. To the best of the authors' knowledge, there are no studies conducted demonstrating the use of graphene in reflectarray for beam-steering applications where graphene is used as a phase-shifting element. The objective of this study is to analyse the capacity of graphene when it is used as a tunable element in a unit cell with typical dimensions of $\lambda/2$. This paper describes the application of graphene for the electronically controllable reconfigurable reflectarray antenna at 1.025 THz. Therefore, an RRA based on the graphene-metal hybrid unit cells is presented in this study at $\lambda/2$ spatial distance, which realises beam-steering at THz frequencies. Moreover, the presented antenna has the potential to integrate into the development of THz RIS, which is significant for future communication technologies, such as 6G and beyond. The key reason for using this frequency is to design an indoor communication channel with a large bandwidth that is also capable of handling optical channels. The proposed flexible communication system can be seamlessly included in fibre-based network topologies.

2. METHOD

2.1. Modelling of Graphene

Graphene is a single atomic layer of a honeycomb microscopic structure arranged as micro-ribbons [20]. It was first differentiated from graphite by Geim & Novoselov [21]. Graphene possesses unique optical and electric characteristics such as zero-gap band structure, high carrier mobility, and tunability of conductivity against applied bias voltage [22]. Since single atomic layers are two-dimensional, and electronic structures swiftly divert their properties with the number of layers, it was found that 10 layers make graphene a three-dimensional material. Moreover, the graphene structure becomes stable under a typical ambient environment at a scale of 10 nanometres [21]. The graphene was modelled in CST as a 3D material whose dielectric characteristics were defined using Eq. (1) [23]:

$$\varepsilon_g = 1 + i\,\frac{\sigma_g}{\omega d \varepsilon_0} \tag{1}$$

where complex surface conductivity of graphene is expressed by σ_g; ε_0 is the permittivity of space 8.85×10^{-12} F/m; d is the thickness of graphene. Eq. (1) reasserts that the complex permittivity of graphene has a dependence on its thickness, or the number of layers modelled. The conductive dispersive properties of graphene can be accurately defined using Kubo's formula, according to which the conductivity of graphene depends on the ambient temperature, chemical potential, and relaxation time as defined by Eq. (2) [24]:

$$\sigma_g = \frac{ie^2 k_B T}{\pi\hbar^2\left(\omega + i\tau^{-1}\right)} \times \left(\frac{\mu_c}{k_B T} + 2\ln\left(e^{\frac{-\mu_c}{k_B T}} + 1\right)\right) + \frac{ie^2}{4\pi\hbar}\ln\left(\frac{2\left|\mu_c\right| - \hbar\left(\omega + i\tau^{-1}\right)}{2\left|\mu_c\right| + \hbar\left(\omega + i\tau^{-1}\right)}\right) \tag{2}$$

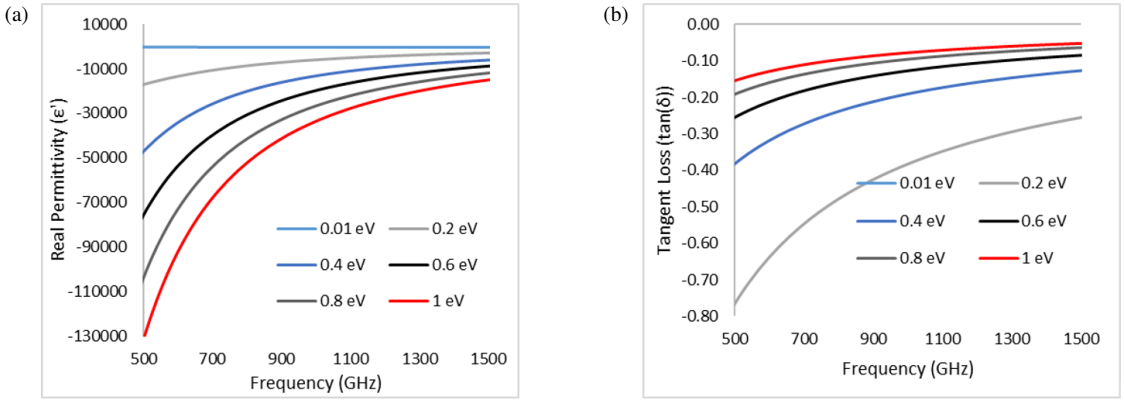

FIGURE 1. (a) Real and (b) imaginary permittivity of graphene.

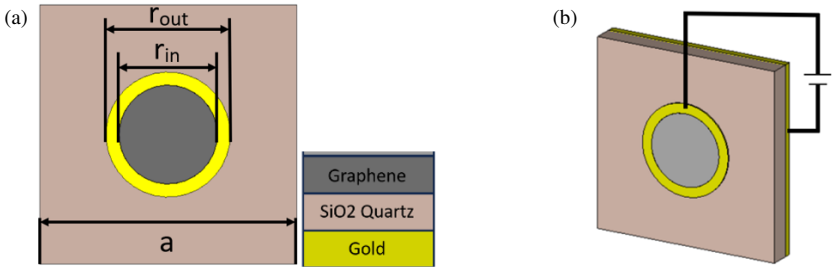

FIGURE 2. Gold-graphene hybrid structure (a) unit cell's top view and (b) biasing setup for the proposed design.

where τ is the free electron relaxation time, μ_c the chemical potential, T the temperature, $\hbar$ the Reduced Planck's constant, ω the angular frequency, and kB the Boltzmann's constant. The relationship between chemical potential and relaxation time can be defined with Eq. (3) [23]:

$$\tau = \left| \frac{\mu_c \mu_n}{v_f^2} \right| \tag{3}$$

where τ is the free electron relaxation time, μ_c the chemical potential, μ_n the electron mobility, whose maximum reported value is 30,000 $cm^2/V{\cdot}s$ for unsuspended graphene [25], and v_f the Fermi velocity with the value of 1.2×10^6 m/s [26]. Here (3) can be simplified as Eq. (4):

$$\tau = 2.08 \times \mu_c \times 10^{-12} \tag{4}$$

Figure 1 presents the graphene's real permittivity and tangent loss at different levels of Fermi energy. With the increase in graphene's Fermi energy, the permittivity decreases, and the tangent loss increases. The Fermi energy of graphene, which is also known as graphene's chemical potential, can be controlled via applied voltage as described by Eq. (5) [27]:

$$V = V_0 + \frac{te\mu_c^2}{\varepsilon_0 \varepsilon_r \pi \hbar^2 V_f^2} \tag{5}$$

Here, V_0 represents the voltage caused by graphene's natural doping (considered zero), t the substrate thickness, e the electronic charge in Statcoulomb, and ε_0 the free space permittivity.

2.2. Unit Cell Design

The schematic diagram of a proposed unit cell of RRA is shown in Fig. 2(a). The metallic patch and full ground plane are formed of gold with a conductivity of 4.6×10^7 S/m with a thickness (t) of 1 µm. In addition, the graphene with a thickness (gt) of 0.01 µm is modelled inside the ring of gold. A substrate of SiO_2 Quartz is used with a permittivity (ε_r) of 3.75 and a tangent loss (δ) of 0.0004. The dielectric spacer thickness, h, is 15 µm, which is at 0.05λ scale for an acceptable trade-off between phase linearity and resonance efficiency [28]. The lattice constant, a is modelled of 136 µm length and width corresponding to less than 0.5λ at the desired frequency, so that grating lobes can be avoided [2]. In addition, the radius (r_{in}) of the graphene patch inside the gold ring is optimised at 26 µm, and the outer radius of the gold ring (r_{out}) is 33 µm, which means that the width of the gold ring (w) was set to 7 µm for the best phase coverage and resonance efficiency.

The surface conductivity of graphene, which is related to the permittivity of graphene, can be tuned by using the top gate configuration of an ion-gel, which freely modulates the Fermi energy between 0.01 eV and 1.0 eV. In this common approach, the Fermi energy of graphene is controlled by the applied voltage [29]. An ion gel layer of 0.99 µm thickness and 1.82 permittivity on the top layer graphene surface is added to the unit cell as shown in Fig. 2(b). This technique of biasing each unit cell of graphene is inspired by [30] as the periodically arranged graphene patches are disconnected from each other. Therefore, ion gel plays a significant role in the most efficient dielectric for tuning graphene plasmons. It must be recalled that the re-

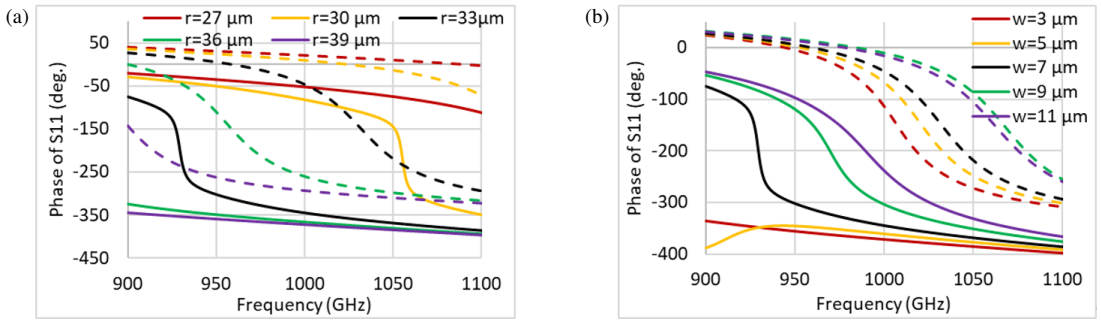

FIGURE 3. (a) Reflection coefficient phase at 0.01 eV (—) and 1.0 eV (- - -) versus unit cell dimensions (a) r and (b) w.

laxation time also varies in graphene with the changes in chemical potential as shown in Eq. (4). Therefore, variation in the permittivity according to chemical potential implies that the relaxation time is also varied simultaneously.

The possible fabrication process of the designed RRA can be completed in two stages. In the first stage, gold (Au) is fabricated, which is possible through lithography [31]. Using photolithography and thermal evaporation, metasurface absorbers are fabricated at a nanometer scale [32]. The fabrication of gold can be completed efficiently through wet etching. At first, a 1 μm thick layer of gold is splutter-coated onto the substrate, which is quartz (SiO_2 in this study). Later, a photoresist layer is created that is spin-coated, exposed to UV and treated to a defined structure (ring in this study). The outside structure is then removed through wet etching using an acidic solution. Finally, acetone is used to remove any remaining photoresist. In the second stage, a graphene film is created. Graphene can be fabricated to complete the design process. Among several methods of producing nanomaterials, the chemical vapour deposition (CVD) technique has been effective in producing single-layer graphene. Copper (Cu) is typically used as a metal catalyst substrate for the growth of CVD graphene [33]. The growth of CVD graphene starts when precursor molecules collide with the Cu surface. Subsequently, they are absorbed into the copper's surface, followed by partial or total dehydrogenation of molecules. Finally, the active species are diffused over the surface of copper, which forms the basis of the growth of graphene [34]. Later, graphene is transferred from copper to the desired substrate following either direct transfer (polymer-free) or a poly-methyl methacrylate-assisted method [35].

2.3. Tuning of Unit Cell

Initially, a parametric study was conducted, in which optimum dimensions for the ring were determined. As the required phase difference between multiple states of the unit cell phase in designing of reconfigurable reflectarray is typically 180° [36], the radius (r) of the ring was varied from 27 μm to 39 μm. The resonance moved to a lower frequency as the radius of the ring increased. The objective of this procedure was to find out the radius of the ring where the maximum difference of the reflection coefficient phase (more than 180°) is obtained at our desired frequency range (1025 GHz). Fig. 3 shows the reflection coefficient of the unit cell at two different states by changing graphene's Fermi energy from the lowest possible to the maximum possible value (0.01 eV to 1.0 eV) for different parameters of the unit cell. The solid lines represent graphene's Fermi energy of 0.01 eV, and the dotted lines represent 1.0 eV. From Fig. 3(a), it is evident that the reflection coefficient phase difference is maximum between the two states when $r = 33$ μm at our desired range of frequency. Another parameter, which is the difference between r_{in} and r_{out} (w) was also varied from 3 μm to 11 μm. It can be seen from Fig. 3(b) that the optimum phase difference at 1025 GHz is obtained when the value of w is equal to 7 μm.

The analysis of the electric field in the unit cell is important to fine-tuning the resonant frequency and the corresponding phase. Moreover, analysing the electric field distribution gives an insight into the radiation characteristics of the reflectarray's element designed with graphene. It increases the importance of the near electric field distribution within the graphene-gold unit cell at a frequency of 1025 GHz, where the reflection phase change between the two states of graphene is maximum. The electric field distribution of the element is shown in Fig. 4. The maximum E-field distribution in the case of graphene's Fermi energy 0.01 eV is found to be 1.6×10^7 V/m, and it is found to be 9.2×10^6 V/m in the case of 1.0 eV. Moreover, the unit cell near the conducting patch also shows a decrease in E-field distribution when graphene's Fermi energy is increased from 0.01 to 1.0 eV. It can also be seen that the E-field pattern provides 2 half variations in the case of 0.01 eV in the direction of the y-axis. The E-field travels in such a way that the direction is downward-upward and downward from top to bottom. However, the direction is opposite in the case of 1.0 eV, where it is upward-downward and upward. This observation validates the phenomenon behind the change in the reflection coefficient phase at the frequency of 1025 GHz.

3. DESIGN OF RRA

A reflectarray antenna generally collimates the incoming wave fed by a horn antenna and generates a planar phase front, a high-gain pencil beam. Using graphene, beam steering can be realised by tuning the phase of reflecting elements independently. It is worth noticing that the maximum phase deviation with changes in chemical potential is obtained at 1025 GHz when r_{out} is 33 μm, and r_{in} is 26 μm. Fig. 5 shows that the S_{11} amplitude is better than −3 dB (0.7 magnitude) at 1025 GHz when

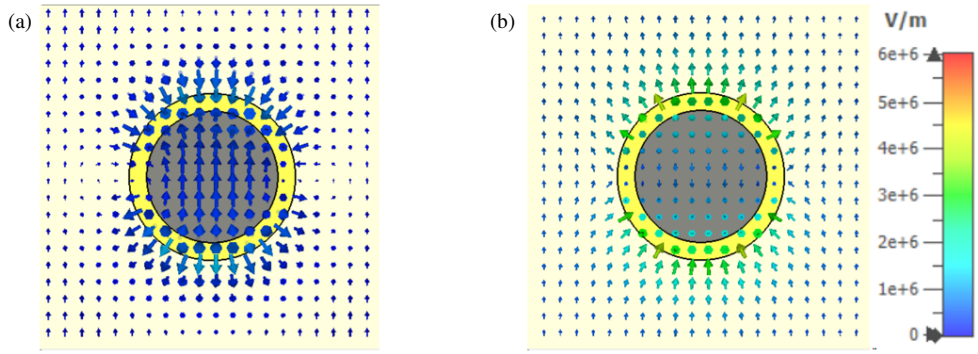

FIGURE 4. E-field distribution when graphene's Fermi energy is (a) 0.01 eV and (b) 1.0 eV.

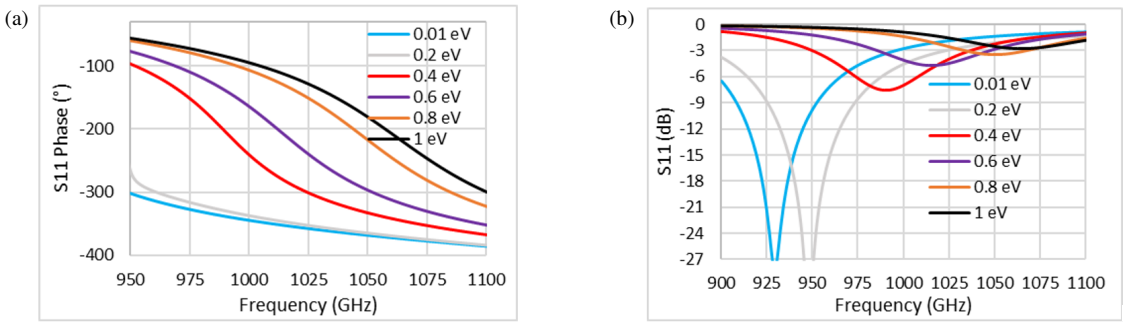

FIGURE 5. Reflection coefficient (a) phase and (b) magnitude at graphene's different chemical potential.

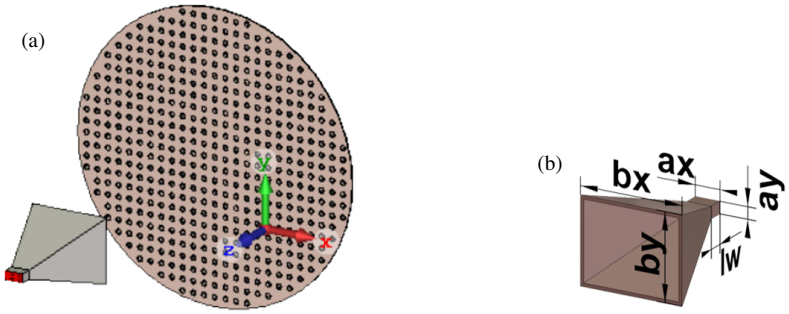

FIGURE 6. (a) Reflectarray design with feed antenna and (b) feed antenna design (with dimensions $ax = 168\,\mu$m, $ay = 47\,\mu$m, $bx = 881\,\mu$m, $by = 715\,\mu$m, $lw = 136\,\mu$m).

the chemical potential is 0.01 or 1.0 eV. However, values of eV between 0.01 and 1.0 show higher losses in reflection coefficients. Since the optimum phase shift for designing a reconfigurable reflectarray should be greater than 180° [37], and the magnitude required is no less than 0.7 [38]; therefore, to a reconfigurable reflectarray, chemical potential values of 0.01 and 1.0 eV were chosen.

Figure 6(a) represents the reflectarray designed at a diameter of 3.4 mm, which comprises a maximum of 25 elements on its line of diameter. The array was excited by the pyramidal horn antenna, which is shown in Fig. 6(b). The wall thickness of the feed antenna is 30 µm, and the horn length is 1198 µm. It should be noted that the antenna elements at the array's edges are illuminated by the -10 dB gain of the feed [1]. The -10 dB beamwidth of the feed antenna is 52°, and the angle created from the feed centre of the horn antenna to the edges of the array is also 52°. Therefore, the focal length to diameter (F/D) ratio in this case needs to be 1, which implies that the feed antenna is positioned at the same distance as the diameter of the antenna.

4. BEAM STEERING ANALYSIS AND DISCUSSION

The required phase shift of each element can be calculated using Eq. (6) [39].

$$\Phi = -k_0 \left(R_i - \sin\theta \left(x_i \cos\varphi + y_i \sin\varphi\right)\right) \tag{6}$$

where Φ is the phase required for each unit cell; k_0 is the wave number; x_i and y_i are the position coordinates of the unit cell; θ and φ define the reflection beam direction; R_i is the distance of the ith element from the phase centre of the feed antenna. The required phase needs to be quantised when a 1-bit RRA is de-

FIGURE 7. (a) Phase distribution of RRA and (b) its 1-bit quantisation.

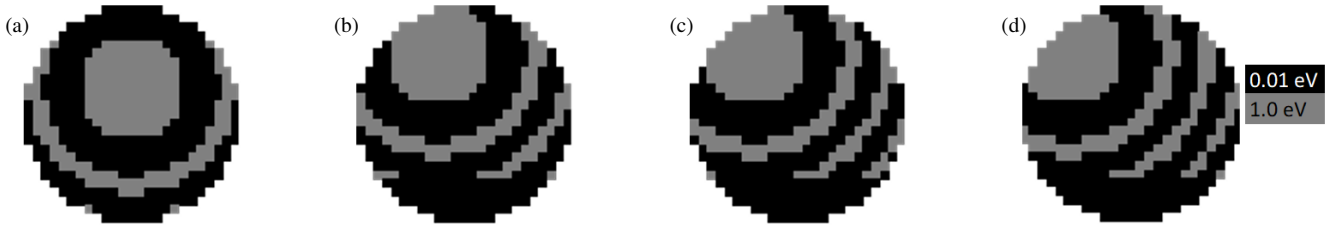

FIGURE 8. Phase distribution of RRA at 1025 GHz for beam reflection at (a) $(\theta, \varphi) = (6°, 90°)$, (b) (14°, 116°), (c) (17°, 127°) and (d) (19°, 138°).

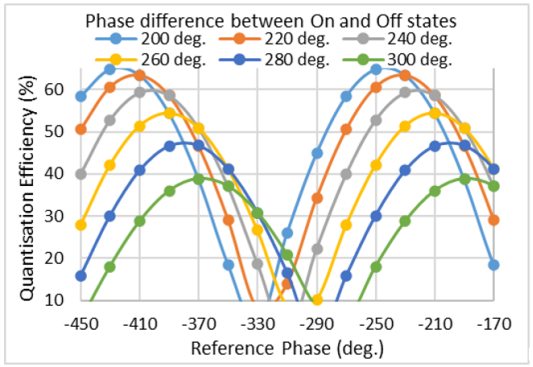

FIGURE 9. Quantisation efficiency versus reference phase for different phase differences.

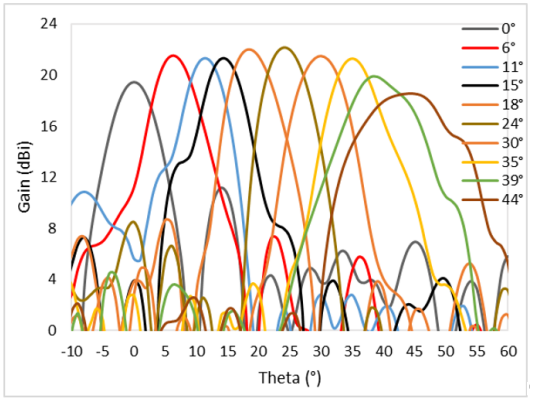

FIGURE 10. Co-polarized radiation beam at 1025 GHz for a phi angle (φ) of 90°.

signed. Therefore, the progressive phase required is quantised as given by Eq. (7).

$$\Phi = \begin{cases} -160°, & 1.0\,\text{eV}, \\ 0°, & 0.01\,\text{eV}, \end{cases} \quad \begin{matrix} -100 > \Phi > -240 \\ \text{Otherwise} \end{matrix} \tag{7}$$

Figure 7(a) shows the configuration of the progressive phase for the beam reflection at $(\theta, \varphi) = (0°, 0°)$ calculated using Eq. (6). The 1-bit quantised phase distribution is shown in Fig. 7(b) where black areas represent the graphene's chemical potential of 0.01 eV (Off state) while grey area represents the graphene's chemical potential of 1.0 eV (On state).

In order to optimise the quantisation so that the array suffers from minimal quantisation losses, quantisation efficiency was calculated using Eq. (8) [40].

$$\eta_q = \frac{|\text{AF}(\theta, \varphi)_{1-\text{bit}}|^2}{|\text{AF}(\theta, \varphi)_{\text{continuous}}|^2} \tag{8}$$

Figure 8 represents the quantisation efficiency of a 1-bit configuration where the primary phase of the reflection coefficient was varied from $-170°$ to $-450°$, and quantisation efficiency was determined for phase differences between On and Off states ranging from 200° to 300° at steps of 20°. Based on the phase of unit cell at On and Off states as provided in Eq. (7), the quantisation efficiency is found to be 50%.

There were more than 10 configurations of phase distribution created for beam steering. Fig. 9 shows the phase distributions of RRA to steer the beam in the direction of $(\theta, \varphi) = (6°, 90°), (14°, 116°), (17°, 127°)$ and (19°, 138°).

Figure 10 shows the co-polarized radiation pattern at different theta (θ) and phi $(\varphi) = 90°$. The maximum gain obtained was 21.5 dBi. This configuration is proficient in offset medium. The side-lobe levels in all the radiation patterns are found to be below -10 dB except at 44° and 0°, where it is found to be greater than -10 dB. Moreover, the main lobe gain is even with the change in main lobe direction at theta until 35°. Maximum gain tends to reduce below 20 dBi when the scan angle is over 40°. To give further insight into the radiation patterns with the main lobe direction at different angles, the 3D far-field patterns of the designed RRA with three different main lobe directions are presented at 1025 GHz in Fig. 11. It should be noted that the radiation patterns shown in Figs. 11(a), 11(b), 11(c), and 11(d)

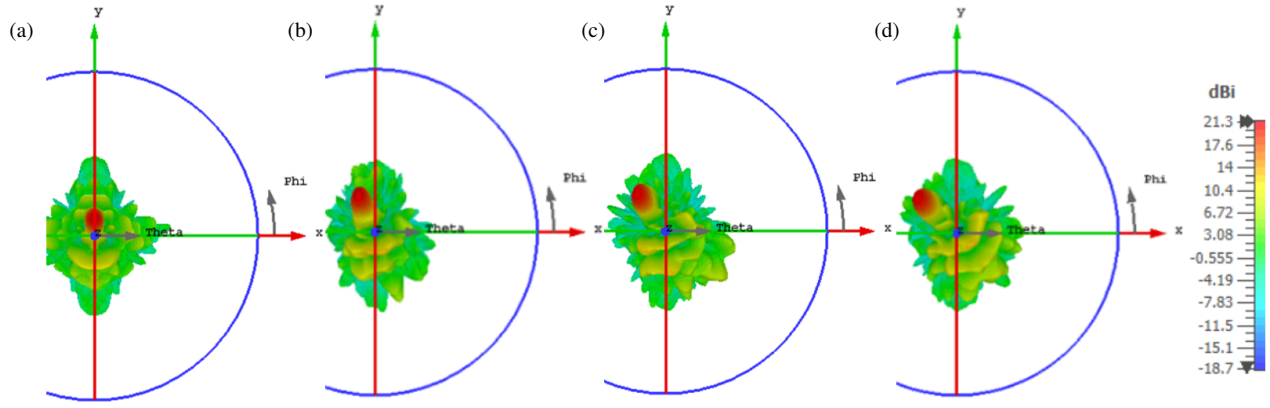

FIGURE 11. Simulated 3-D far-field radiation patterns at $(\theta, \varphi) =$ (a) (6°, 90°), (b) (14°, 116°), (c) (17°, 127°) and (d) (19°, 138°).

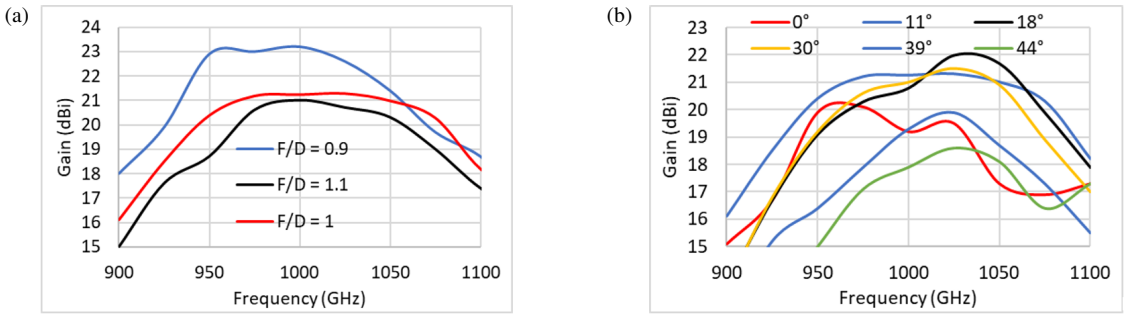

FIGURE 12. Gain over frequency against (a) different F/D ratios and (b) different beam-steering angles.

TABLE 1. Main performance parameters of proposed RRA.

Beam direction		Main lobe (dBi)	SLL (dB)	3 dB beamwidth (°)
θ(°)	φ(°)			
0	90	19.3	−8.3	6.7
6	90	21.3	−10.6	6.4
11	90	21.3	−10.1	6
18	90	22	−13.3	6.9
24	90	22.2	−12.2	6.7
30	90	21.5	−14	7.5
35	90	21.3	−11.4	7
39	90	19.9	−11	10.9
44	90	18.6	−9.2	14.4
14	116	20.8	−10	6.9
17	127	21	−12.2	6.9
19	138	21.2	−12.3	6.6

correspond to the phase distribution represented in Figs. 9(a), 9(b), 9(c), and 9(d), respectively.

Moreover, the bandwidth of the designed RRA at an offset of 11° was calculated as shown in Fig. 12(a) at different F/D ratios. The simulated −1 dB bandwidth is achieved between 950 GHz and 1075 GHz, which makes 12.2% for the centre frequency of 1025 GHz. For this analysis, the F/D ratio was also varied from 0.9 to 1.1. It was realised that the maximum gain increases when the F/D ratio is 0.9. However, −1 dB bandwidth decreases to 9.7% (940 GHz to 1040 GHz). An analysis of beam-steering bandwidth was also performed in which the peak gain was measured at different steered angles as shown in Fig. 12(b). The peak gain stays over 19 dBi from 950 GHz to 1075 GHz for steered beams at 11°, 18°, and 30°. This shows that the proposed RRA can steer the beam in a wide range of frequencies. However, the bandwidth of the array seems to be reduced when the steering angle is over 39°, after which the array's bandwidth is narrowed down to its operating frequency. A summary of the main performance parameters is presented in Table 1. A comparison of the proposed RRA tuned by graphene is made with the other RRAs tuned with phase shifters such as PIN diode and liquid crystals, in Table 2. In [41], the phase control was linear using LC at 23.8 GHz, and the unit cell was designed at $0.4\lambda \times 0.3\lambda$ dimensions. The RRA showed a maximum gain of 18 dBi with an aperture efficiency of 5.8%. A complete 360° phase shift was possible in [42] with the help of two PIN diodes. The performance was found to be extraordinary in terms of aperture efficiency and side lobe level. The operation of other phase shifters does not exceed their application at over 200 GHz. The maximum frequency at which liquid crystal was used recently for designing RRA was 115 GHz [1]. Although most applications of graphene are related to absorbers, and it is considered a lossy material, its combination with the pure metallic material offers extraordinary characteristics in designing reconfigurable reflectarrays. Nevertheless, the losses incurred due to graphene can be reduced by decreasing the area covered by graphene in the hybrid unit cell. The geometry of the unit cell can be optimised to further reduce the reflection

TABLE 2. Performance comparison of RRAs with proposed RRA based on the hybrid structure of gold and graphene.

Ref.	Frequency (GHz)	Unit cell size	Phase shifter	SLL (dB)	Beam steering	Aperture efficiency	1-dB B.W
[1]	115	$\lambda/2$	LC	-8.4	20°	-	-
[41]	23.8	0.4λ	LC	-15	110°	5.8%	12%
[42]	26.1	0.43λ	PIN Diode	-17.7	110°	27.1%	5%
[10]	108	$\lambda/2$	LC	-14.8	90°	15%	
[7]	10	$\lambda/2$	PIN Diode	-12	90°	-	15%
[6]	10	$\lambda/2$	PIN Diode	-	12°	-	30%
[16]	1600	$\lambda/16$	Graphene	-	-	6.2%	-
[19]	1500	$\lambda/2$	Graphene	-5.4	-	2%	-
This work	1025	$\lambda/2$	Graphene	-10	80°	11%	12%

loss and at the same time ensure that the phase difference obtained is optimum for designing RRA. Moreover, graphene's resistive losses can also be reduced by insulating the graphene with insulating materials. Graphene is designed for RRA to get vortex waves in [16], where the unit cells were designed at $\lambda/16$ dimensions. Compared to other RRAs, the aperture efficiency of the proposed hybrid structure of 11% is satisfactory. In [19], the graphene-based unit cell was designed at $\lambda/2$ dimensions. However, it showed the performance of graphene being used as the main conducting element for beamforming in reflectarray, which showed very small aperture efficiency. Even though the plasmonic nature of graphene is compelled to resonate at a very small fraction of the wavelengths, its use as the phase delay component also gives satisfactory results. These characteristics of the proposed hybrid structure give insight into the potential use of graphene as a phase delay component in the development of RIS for future generations of telecommunication, such as 6G and 7G.

5. CONCLUSION

A hybrid of graphene and metallic structure is modelled in this paper for designing an RRA. Graphene is modelled as a 3D material in CST Studio with a thickness of 10 nm. 1-bit RRA is simulated on a 3.4 mm circular aperture. The graphene material in a hybrid structure performs extraordinarily at THz frequencies with sufficient aperture efficiency and bandwidth. Therefore, graphene tends to advance the designing of RRAs at THz frequencies. This type of reflectarray modelled with gold and graphene is novel, and its beam-steering capacity is most suitable for applications of RIS operating in the THz band.

ACKNOWLEDGEMENT

This work is funded by the Ministry of Higher Education (MoHE) Malaysia under the Fundamental Research Grant Scheme Vot No. FRGS/1/2021/TK0/UTHM/02/19 and No. FRGS/1/2023/TK07/UTEM/02/7, and it is partially sponsored by Universiti Tun Hussein Onn Malaysia (UTHM). The author would also like to thank the Staff of UTHM and UTeM for technical support.

REFERENCES

[1] Yang, J., P. Wang, S. Sun, Y. Li, Z. Yin, and G. Deng, "A novel electronically controlled two-dimensional terahertz beam-scanning reflectarray antenna based on liquid crystals," *Frontiers in Physics*, Vol. 8, 576045, Oct. 2020.

[2] You, X., R. T. Ako, W. S. L. Lee, M. X. Low, M. Bhaskaran, S. Sriram, C. Fumeaux, and W. Withayachumnankul, "Terahertz reflectarray with enhanced bandwidth," *Advanced Optical Materials*, Vol. 7, No. 20, 1900791, 2019.

[3] Niu, T., W. Withayachumnankul, B. S.-Y. Ung, H. Menekse, M. Bhaskaran, S. Sriram, and C. Fumeaux, "Experimental demonstration of reflectarray antennas at terahertz frequencies," *Optics Express*, Vol. 21, No. 3, 2875–2889, Feb. 2013.

[4] Imaz-Lueje, B., D. R. Prado, M. Arrebola, and M. R. Pino, "Reflectarray antennas: A smart solution for new generation satellite mega-constellations in space communications," *Scientific Reports*, Vol. 10, No. 1, 21554, 2020.

[5] Encinar, J. A., R. Florencio, M. Arrebola, M. A. S. Natera, M. Barba, J. E. Page, R. R. Boix, and G. Toso, "Dual-polarization reflectarray in Ku-band based on two layers of dipole arrays for a transmit-receive satellite antenna with South American coverage," *International Journal of Microwave and Wireless Technologies*, Vol. 10, No. 2, 149–159, Mar. 2018.

[6] Abbasi, M. I., M. Y. Ismail, and M. R. Kamarudin, "Development of a pin diode-based beam-switching single-layer reflectarray antenna," *International Journal of Antennas and Propagation*, Vol. 2020, No. 1, 8891759, Dec. 2020.

[7] Luyen, H., Z. Zhang, J. H. Booske, and N. Behdad, "Wideband, beam-steerable reflectarray antennas exploiting electronically reconfigurable polarization-rotating phase shifters," *IEEE Transactions on Antennas and Propagation*, Vol. 70, No. 6, 4414–4425, 2022.

[8] Nam, I.-J., S. Lee, and D. Kim, "Miniaturized beam reconfigurable reflectarray antenna with wide 3-D beam coverage," *IEEE Transactions on Antennas and Propagation*, Vol. 70, No. 4, 2613–2622, Apr. 2022.

[9] Perruisseau-Carrier, J. and A. K. Skrivervik, "Monolithic MEMS-based reflectarray cell digitally reconfigurable over a 360° phase range," *IEEE Antennas and Wireless Propagation Letters*, Vol. 7, 138–141, 2008.

[10] Meng, X., M. Nekovee, and D. Wu, "The design and analysis of electronically reconfigurable liquid crystal-based reflectarray metasurface for 6G beamforming, beamsteering, and beamsplitting," *IEEE Access*, Vol. 9, 155 564–155 575, 2021.

[11] Yang, J., L. Xu, G. Zhang, R. Mao, Z. Yin, H. Lu, G. Deng, and Y. Li, "Active continuous control of terahertz wave based on a reflectarray element-liquid crystal-grating electrode hybrid structure," *Optics Express*, Vol. 30, No. 10, 17 361–17 370, 2022.

[12] Carrasco, E. and J. Perruisseau-Carrier, "Reflectarray antenna at terahertz using graphene," *IEEE Antennas and Wireless Propagation Letters*, Vol. 12, 253–256, 2013.

[13] Capaz, R. B., "Grand challenges in graphene and graphite research," *Frontiers in Carbon*, Vol. 1, Oct. 2022.

[14] Shi, L. P., Q. H. Zhang, S. H. Zhang, C. Yi, and G. X. Liu, "Efficient graphene reconfigurable reflectarray antenna electromagnetic response prediction using deep learning," *IEEE Access*, Vol. 9, 22 671–22 678, 2021.

[15] Singh, A., M. Andrello, E. Einarsson, N. Thawdar, and J. M. Jornet, "Design and operation of a smart graphene-metal hybrid reflectarray at THz frequencies," in *2020 14th European Conference on Antennas and Propagation (EuCAP)*, 1–5, Copenhagen, Denmark, Mar. 2020.

[16] Chang, Z., B. You, L.-S. Wu, M. Tang, Y.-P. Zhang, and J.-F. Mao, "A reconfigurable graphene reflectarray for generation of vortex THz waves," *IEEE Antennas and Wireless Propagation Letters*, Vol. 15, 1537–1540, 2016.

[17] Deng, L., Y. Zhang, J. Zhu, and C. Zhang, "Wide-band circularly polarized reflectarrayusing graphene-based pancharatnam-berry phase unit-cells for terahertz communication," *Materials*, Vol. 11, No. 6, 956, 2018.

[18] Zainud-Deen, S. H., A. M. Mabrouk, and H. A. Malhat, "Frequency tunable graphene metamaterial reflectarray," *Wireless Personal Communications*, Vol. 103, 1849–1857, 2018.

[19] Hassan, A. A., R. R. Elsharkawy, D. A. Saleeb, E.-S. M. El-Rabie, and A. S. Elkorany, "Single-beam graphene reflectarray for terahertz band communication," *Analog Integrated Circuits and Signal Processing*, Vol. 112, No. 3, 517–525, 2022.

[20] Alaee, R., M. Farhat, C. Rockstuhl, and F. Lederer, "A perfect absorber made of a graphene micro-ribbon metamaterial," *Optics Express*, Vol. 20, No. 27, 28 017–28 024, 2012.

[21] Geim, A. K. and K. S. Novoselov, "The rise of graphene," *Nature Materials*, Vol. 6, No. 3, 183–191, Mar. 2007.

[22] Xiao, B., M. Gu, K. Qin, and S. Xiao, "Absorption enhancement in graphene with an efficient resonator," *Optical and Quantum Electronics*, Vol. 49, 1–8, 2017.

[23] Armaghani, S., S. Khani, and M. Danaie, "Design of all-optical graphene switches based on a Mach-Zehnder interferometer employing optical Kerr effect," *Superlattices and Microstructures*, Vol. 135, 106244, 2019.

[24] Zhou, R., T. Jiang, Z. Peng, Z. Li, M. Zhang, S. Wang, L. Li, H. Liang, S. Ruan, and H. Su, "Tunable broadband terahertz absorber based on graphene metamaterials and VO_2," *Optical Materials*, Vol. 114, 110915, 2021.

[25] Bolotin, K. I., K. J. Sikes, Z. Jiang, M. Klima, G. Fudenberg, J. Hone, P. Kim, and H. L. Stormer, "Ultrahigh electron mobility in suspended graphene," *Solid State Communications*, Vol. 146, No. 9-10, 351–355, 2008.

[26] Jiao, Z. and H. J. W. Zandvliet, "Determination of the Fermi velocity of graphene on MoS_2 using dual mode scanning tunneling spectroscopy," *Applied Physics Letters*, Vol. 118, No. 16, 2021.

[27] Yadav, R., V. S. Pandey, and P. Verma, "Nano-scaled graphene plasmonic-based vanadium dioxide Yagi-Uda array MIMO antenna for terahertz applications," *Plasmonics*, Vol. 19, 3345–3358, 2024.

[28] Bansal, R., "Antenna theory; Analysis and design," *Proceedings of the IEEE*, Vol. 72, No. 7, 989–990, Jul. 1984.

[29] Wang, T., Y. Zhang, H. Zhang, and M. Cao, "Dual-controlled switchable broadband terahertz absorber based on a graphene-vanadium dioxide metamaterial," *Optical Materials Express*, Vol. 10, No. 2, 369–386, 2020.

[30] Ghosh, S. K., S. Das, and S. Bhattacharyya, "Graphene-based metasurface for tunable absorption and transmission characteristics in the near mid-infrared region," *IEEE Transactions on Antennas and Propagation*, Vol. 70, No. 6, 4600–4612, Jun. 2022.

[31] Wang, B., A. Sadeqi, R. Ma, P. Wang, W. Tsujita, K. Sadamoto, Y. Sawa, H. R. Nejad, S. Sonkusale, C. Wang, M. Kim, and R. Han, "Metamaterial absorber for THz polarimetric sensing," in *Terahertz, RF, Millimeter, and Submillimeter-Wave Technology and Applications XI*, Vol. 10531, 170–176, Feb. 2018.

[32] Du, Y., W. Wei, X. Zhang, and Y. Li, "Tuning metamaterials nanostructure of Janus gold nanoparticle film for surface-enhanced Raman scattering," *The Journal of Physical Chemistry C*, Vol. 122, No. 14, 7997–8002, Apr. 2018.

[33] Saeed, M., Y. Alshammari, S. A. Majeed, and E. Al-Nasrallah, "Chemical vapour deposition of graphene — Synthesis, characterisation, and applications: A review," *Molecules*, Vol. 25, No. 17, 3856, Aug. 2020.

[34] Hernández, A. R. R., A. G. Cruz, and J. Campos-Delgado, "Chemical vapor deposition synthesis of graphene on copper foils," in *Graphene — A Wonder Material for Scientists and Engineers*, IntechOpen, 2023.

[35] Wu, Z., X. Zhang, A. Das, J. Liu, Z. Zou, Z. Zhang, Y. Xia, P. Zhao, and H. Wang, "Step-by-step monitoring of CVD-graphene during wet transfer by Raman spectroscopy," *RSC Advances*, Vol. 9, No. 71, 41 447–41 452, 2019.

[36] Pei, X., H. Yin, L. Tan, L. Cao, Z. Li, K. Wang, K. Zhang, and E. Björnson, "RIS-aided wireless communications: Prototyping, adaptive beamforming, and indoor/outdoor field trials," *IEEE Transactions on Communications*, Vol. 69, No. 12, 8627–8640, 2021.

[37] Xi, B., Y. Xiao, K. Zhu, Y. Liu, H. Sun, and Z. Chen, "1-bit wideband reconfigurable reflectarray design in Ku-band," *IEEE Access*, Vol. 10, 4340–4348, 2021.

[38] Chang, Z., B. You, L.-S. Wu, M. Tang, Y.-P. Zhang, and J.-F. Mao, "A reconfigurable graphene reflectarray for generation of vortex THz waves," *IEEE Antennas and Wireless Propagation Letters*, Vol. 15, 1537–1540, 2016.

[39] Huang, J. and J. A. Encinar, "Reflectarray antennas," in *Encyclopedia of RF and Microwave Engineering*, John Wiley & Sons, Inc., Hoboken, NJ, USA, 2007.

[40] Lee, S.-G., Y.-H. Nam, Y. Kim, J. Kim, and J.-H. Lee, "A wide-angle and high-efficiency reconfigurable reflectarray antenna based on a miniaturized radiating element," *IEEE Access*, Vol. 10, 103 223–103 229, Sep. 2022.

[41] Zhang, W., Y. Li, and Z. Zhang, "A reconfigurable reflectarray antenna with an 8 µm-thick layer of liquid crystal," *IEEE Transactions on Antennas and Propagation*, Vol. 70, No. 4, 2770–2778, Apr. 2022.

[42] Wang, E., G. Peng, K. Zhong, F. Wu, Z. H. Jiang, R. Sauleau, and W. Hong, "A 1296-Cell reconfigurable reflect-array antenna with 2-bit phase resolution for Ka-band applications," *IEEE Transactions on Antennas and Propagation*, Vol. 72, No. 4, 3425–3437, Apr. 2024.